Small-Signal Model Analysis of Droop-controlled Modular Multilevel Converters with Circulating Current Suppressing Controller

J. Freytes[1], G. Bergna[2], J.A. Suul[2,3], S. D'Arco[2], H. Saad[4], X. Guillaud[1]

[1] *Université Lille, Centrale Lille, Arts et Métiers, HEI - EA 2697 - L2EP - Lille, France - e-mail: julian.freytes@centralelille.fr*

[2] *Department of Electric Power Engineering, Norwegian University of Science and Technology - Trondheim, Norway - e-mail: gilbert.bergna@ntnu.no*

[3] *SINTEF Energy Research - Trondheim, Norway - e-mail: jon.a.suul@sintef.no, salvatore.darco@sintef.no*

[4] *Réseau de Transport d'Électricité (RTE) - La Défense, France - e-mail: hani.saad@rte-france.com*

Keywords: HVDC Transmission, Modular Multilevel Converter, State-Space Modelling, Small-Signal Stability Analysis

Abstract

This paper presents a small signal eigenvalue analysis applied to a droop-controlled HVDC terminal based on the Modular Multilevel Converter (MMC) topology. The applied linearised model is derived from previous modelling efforts recently proposed in the literature, which rely on the application of three Park transformations at different frequencies (ω, -2ω and 3ω) applied to associated variables defined within the MMC model. The investigated configuration is controlled under the well-known Circulating Current Suppression Controller (CCSC). The developed small-signal model is utilized to evaluate two different approaches for calculating the insertion index for modulation of the MMC, and to reveal potential stability problems in the system. It is demonstrated by participation factor analysis that the potentially unstable modes of the system under the investigated control strategy are linked to the uncontrolled zero-sequence component of the common-mode current resulting from the CCSC.

1 Introduction

The Modular-Multilevel Converter (MMC) represents the recent development among the diverse available topologies of Voltage Source Converters (VSCs) and is allegedly the most suitable converter solution for HVDC transmission systems [1]. Modelling and control of the MMC can be considered in general as more challenging compared to two- or three-level VSCs, since it is characterized by additional internal dynamics related to the common-mode currents and the distributed capacitor voltages within each of its arms [2]. Furthermore, multiple frequency components naturally appear in the internal variables of the MMC [3]. Thus, it is not possible to obtain and further linearise a Steady-State Time Invariant (SSTI) state-space model in a single Synchronous Reference Frame (SRF), according to the modelling approaches commonly applied for two-level VSCs [4, 5].

In general, state-space models can ensure a flexible framework for controller design and system stability analysis. Most previously developed state-space models representing the internal dynamics of MMCs result in Steady-State Time Periodic (SSTP) models, where the steady-state operation is represented by an orbit in state-space coordinates and not by a constant equilibrium point. Stability analysis of the MMC in SSTP representation was recently studied in [6] by the application of time-periodic system theory (Poincaré multipliers). However, application of traditional eigenvalue-based techniques commonly applied in the power system community depend on an SSTI model where states remain constant in steady state [7]. Thus, accurate SSTI representation and linearization of MMC models is necessary for detailed eigenvalue-based assessment of small-signal stability in AC and DC power networks.

A few SSTI modelling approaches for MMCs have been recently proposed in [8–14]. However, the models from [8–12] rely on simplifications that prevent accurate representation of the internal dynamics characterizing the MMC. On the other hand, the more detailed models presented in [13, 14] are able to represent the particular dynamics of the MMC by following two different approaches. Nevertheless, these publications do not consider the DC side dynamics since they assume constant DC voltage sources.

This paper extends the previous modelling efforts presented in [14], which derived a dynamic nonlinear SSTI model of an MMC with Circulating Current Suppression Controller (CCSC) according to [15]. This extension is achieved, firstly, with the consideration of a simplified DC bus model. Since the DC voltage is assumed as a state-variable, a DC droop controller is considered. Secondly, the complete SSTI model (MMC, DC bus and controllers) is linearised for obtaining a small-signal representation. The stability of the resulting model is analyzed using traditional eigenvalue based methods. The SSTI model is linearized for two different cases, to evaluate the impact of two different approaches for calculating the insertion index for modulation of the MMC. The stability of the resulting models are analyzed by using traditional eigenvalue-based methods to reveal potential stability problems in the system.

This is the accepted version of a paper published in 13th IET International Conference on AC and DC Power Transmission - ACDC 2017
DOI: 10.1049/cp.2017.0016

2 Modeling of MMC

2.1 Arm Averaged Model (AAM) in *abc* frame

The Arm Averaged Model (AMM) of the MMC is recalled in Fig. 1. The model presents one leg for each phase j ($j = a,b,c$), each leg consisting of an upper and a lower arm. Each arm includes an inductance L_{arm}, an equivalent resistance R_{arm} and an aggregated capacitor C_{arm} [16].

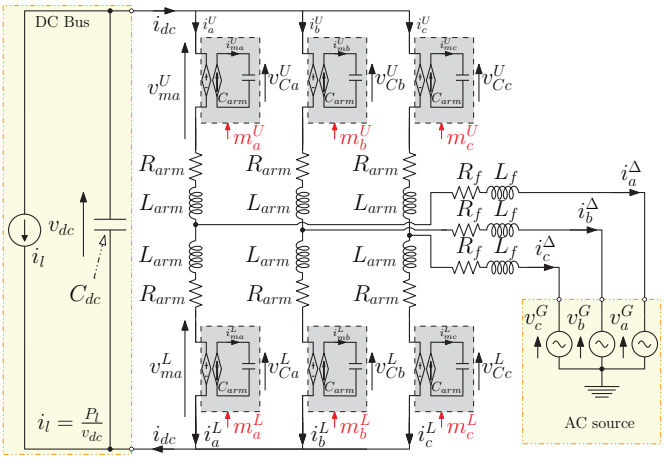

Figure 1: MMC connected to a DC bus capacitor

In the studied system, the simplified dynamics of a DC bus are considered. These dynamics are modeled with an equivalent capacitor C_{dc} which emulates the capacitance of the DC cables and potentially other converter stations connected to the grid. Furthermore, in parallel with C_{dc} there is a controlled current source i_l whose output power is P_l as an equivalent model of the power exchanged in the HVDC system.

Defining $v^{\Delta}_{mj} \stackrel{\text{def}}{=} (-v^{U}_{mj} + v^{L}_{mj})/2$; $v^{\Sigma}_{mj} \stackrel{\text{def}}{=} (v^{U}_{mj} + v^{L}_{mj})/2$ and $i^{\Sigma}_{j} \stackrel{\text{def}}{=} (i^{U}_{j} + i^{L}_{j})/2$, it is possible to derive the currents dynamics of the AAM as follows [14]:

$$L^{ac}_{eq}\frac{di^{\Delta}_{j}}{dt} = v^{\Delta}_{mj} - v^{G}_{j} - R^{ac}_{eq} i^{\Delta}_{j} \tag{1}$$

where $R^{ac}_{eq} = (R_{arm} + 2R_f)/2$ and $L^{ac}_{eq} = (L_{arm} + 2L_f)/2$. The currents i^{Δ}_{j} are oscillating at the grid frequency ω. The common-mode arm currents dynamics are given by:

$$L_{arm}\frac{di^{\Sigma}_{j}}{dt} = \frac{v_{dc}}{2} - v^{\Sigma}_{mj} - R_{arm} i^{\Sigma}_{j} \tag{2}$$

The common-mode arm current i^{Σ}_{j} is mainly composed of a DC component and an AC circulating current at -2ω [14].

The voltages v^{U}_{mj} and v^{L}_{mj}, as well as the currents i^{U}_{mj} and i^{L}_{mj} of each arm j are described by the following equations:

$$v^{U}_{mj} = m^{U}_{j} v^{U}_{Cj}, \quad v^{L}_{mj} = m^{L}_{j} v^{L}_{Cj} \tag{3}$$

$$i^{U}_{mj} = m^{U}_{j} i^{U}_{j}, \quad i^{L}_{mj} = m^{L}_{j} i^{L}_{j} \tag{4}$$

where v^{U}_{mj}, v^{L}_{mj}, i^{U}_{mj} and i^{L}_{mj} are respectively the voltages and currents of the upper and lower arm equivalent capacitors and m^{U}_{j} and m^{L}_{j} are the corresponding instantaneous duty cycles. The voltage and current of the equivalent capacitor are related by the following equation:

$$C_{arm}\frac{dv^{U}_{Cj}}{dt} = i^{U}_{mj}, \quad C_{arm}\frac{dv^{L}_{Cj}}{dt} = i^{L}_{mj}. \tag{5}$$

The addition and difference of the terms in (5) yields,

$$2C_{arm}\frac{dv^{\Sigma}_{Cj}}{dt} = m^{\Delta}_{j}\frac{i^{\Delta}_{j}}{2} + m^{\Sigma}_{j} i^{\Sigma}_{j} \tag{6}$$

$$2C_{arm}\frac{dv^{\Delta}_{Cj}}{dt} = m^{\Sigma}_{j}\frac{i^{\Delta}_{j}}{2} + m^{\Delta}_{j} i^{\Sigma}_{j} \tag{7}$$

where $m^{\Delta}_{j} \stackrel{\text{def}}{=} (m^{U}_{j} - m^{L}_{j})$, $m^{\Sigma}_{j} \stackrel{\text{def}}{=} (m^{U}_{j} + m^{L}_{j})$, $v^{\Delta}_{Cj} \stackrel{\text{def}}{=} (v^{U}_{Cj} - v^{L}_{Cj})/2$ and $v^{\Sigma}_{Cj} \stackrel{\text{def}}{=} (v^{U}_{Cj} + v^{L}_{Cj})/2$. A frequency analysis can be performed by assuming that m^{U}_{j} is phased shifted approximately 180° with respect to m^{L}_{j} (where m^{U}_{j} and m^{L}_{j} have a DC component of 0.5 and an oscillating component), resulting in $m^{\Sigma}_{j} \approx 1$ and $m^{\Delta}_{j} \approx \hat{m}cos(\omega t)$. By inspecting the right-side of (6), it can be seen that in steady-state, the first product $m^{\Delta}_{j} i^{\Delta}_{j}$ oscillates at 2ω while the second product $m^{\Sigma}_{j} i^{\Sigma}_{j}$ gives a DC value in the case CCSC is used or a 2ω signal otherwise, resulting for both cases in 2ω oscillations in v^{Σ}_{Cj}. Similarly for v^{Δ}_{Cj}, the first product on the right-side of (7), $m^{\Sigma}_{j} i^{\Delta}_{j}$, oscillates at ω, while the second product $m^{\Delta}_{j} i^{\Sigma}_{j}$ oscillates at ω in the case the CCSC is used or will result in a signal oscillating at ω superimposed to one at 3ω otherwise.

2.2 State space modelling in rotating frame using voltage-based formulations in Σ-Δ representation

This section summarizes the time-invariant model of the MMC with voltage-based formulation as proposed in [14]. To achieve time invariance, first the MMC variables are classified into "Σ" and "Δ" variables. In steady state, the "Δ" variables are oscillating at the grid's angular frequency ω; while "Σ" variables oscillate at -2ω. This is summarized in Table 1.

Variables oscillating at ω	Variables oscillating at -2ω
$i^{\Delta}_{j} = i^{U}_{j} - i^{L}_{j}$	$i^{\Sigma}_{j} = (i^{U}_{j} + i^{L}_{j})/2$
$v^{\Delta}_{mj} = (-v^{U}_{mj} + v^{L}_{mj})/2$	$v^{\Sigma}_{mj} = (v^{U}_{mj} + v^{L}_{mj})/2$
$m^{\Delta}_{j} = m^{U}_{j} - m^{L}_{j}$	$m^{\Sigma}_{j} = m^{U}_{j} + m^{L}_{j}$

Table 1: MMC variables in Σ-Δ representation

To achieve a SSTI model, it is necessary to refer the MMC variables to their corresponding SRFs, following the frequency classification shown in Table 1. For generic variables x^{Σ} and

This is the accepted version of a paper published in 13th IET International Conference on AC and DC Power Transmission - ACDC 2017
DOI: 10.1049/cp.2017.0016

x^{Δ}, time-invariant equivalents are obtained with the Park's transformation defined in the Appendix A as (bold variables means matrix or vectors):

$$\omega^{+} \Rightarrow \boldsymbol{x}^{\boldsymbol{\Delta}}_{\boldsymbol{dqz}} \stackrel{\text{def}}{=} \quad \left[x^{\Delta}_{d}\ x^{\Delta}_{q}\ x^{\Delta}_{z} \right]^{\top} = \boldsymbol{P}_{\omega} \left[x^{\Delta}_{a}\ x^{\Delta}_{b}\ x^{\Delta}_{c} \right]^{\top}$$
$$2\omega^{-} \Rightarrow \boldsymbol{x}^{\boldsymbol{\Sigma}}_{\boldsymbol{dqz}} \stackrel{\text{def}}{=} \quad \left[x^{\Sigma}_{d}\ x^{\Sigma}_{q}\ x^{\Sigma}_{z} \right]^{\top} = \boldsymbol{P}_{\text{-}2\omega} \left[x^{\Sigma}_{a}\ x^{\Sigma}_{b}\ x^{\Sigma}_{c} \right]^{\top}$$

The zero sequences of the vectors in "Δ" representation need additional post processing as they are the only variables that remain time-periodic in steady-state after applying the above transformations. This issue was solved in [14] by means of an auxiliary virtual variable, 90° shifted from the real one, and by using a Park transformation at $+3\omega$ to achieve time invariant signals.

$$3\omega^{+} \Rightarrow \boldsymbol{x}^{\boldsymbol{\Delta}}_{\boldsymbol{Z}} \stackrel{\text{def}}{=} \left[x^{\Delta}_{Z_d}\ x^{\Delta}_{Z_q} \right]^{\top} = \boldsymbol{P}_{3\omega} \left[x^{\Delta}_{z}\ x^{\Delta 90^{\circ}}_{z} \right]^{\top}$$

Using the above definitions, the MMC dynamics in their "$\Sigma - \Delta$" representation can be rewritten in a time-invariant form [14]. The resulting system is recalled in the following.

2.2.1 AC currents

Applying the Park transformation at ω to (1), the time invariant dynamics of the AC side currents $\boldsymbol{i}^{\boldsymbol{\Delta}}_{\boldsymbol{dq}}$ are given as follows:

$$L^{ac}_{eq} \frac{d\boldsymbol{i}^{\boldsymbol{\Delta}}_{\boldsymbol{dq}}}{dt} = -\boldsymbol{v}^{\boldsymbol{G}}_{\boldsymbol{dq}} + \boldsymbol{v}^{\boldsymbol{\Delta}}_{\boldsymbol{mdq}} - R^{ac}_{eq} \boldsymbol{i}^{\boldsymbol{\Delta}}_{\boldsymbol{dq}} - \boldsymbol{J}_{\omega} L^{ac}_{eq} \boldsymbol{i}^{\boldsymbol{\Delta}}_{\boldsymbol{dq}} \tag{8}$$

with $\boldsymbol{J}_{\omega}$ being the cross-coupling matrix at the fundamental frequency as defined in (9),

$$\boldsymbol{J}_{\omega} \stackrel{\text{def}}{=} \begin{bmatrix} 0 & \omega \\ -\omega & 0 \end{bmatrix} \tag{9}$$

$\boldsymbol{v}^{\boldsymbol{G}}_{\boldsymbol{dq}}$ the grid voltage at the point of interconnection and $\boldsymbol{v}^{\boldsymbol{\Delta}}_{\boldsymbol{mdq}}$ the AC-side modulated voltage. This voltage is defined in (10) as a function of the modulation indexes $\boldsymbol{m}^{\boldsymbol{\Delta}}_{\boldsymbol{dq}}$ and $\boldsymbol{m}^{\boldsymbol{\Sigma}}_{\boldsymbol{dqz}}$,

$$\boldsymbol{v}^{\boldsymbol{\Delta}}_{\boldsymbol{mdq}} = \frac{1}{4} \boldsymbol{V}^{\boldsymbol{\Delta}} \left[\boldsymbol{m}^{\boldsymbol{\Delta}}_{\boldsymbol{dq}}, \boldsymbol{m}^{\boldsymbol{\Sigma}}_{\boldsymbol{dq}}, m^{\Sigma}_{z} \right]^{\top}, \tag{10}$$

and $\boldsymbol{V}^{\boldsymbol{\Delta}}$, the following 2×5 time invariant voltage matrix:

$$\boldsymbol{V}^{\boldsymbol{\Delta}} \stackrel{\text{def}}{=} \begin{bmatrix} -2v^{\Sigma}_{Cz} - v^{\Sigma}_{Cd}; & v^{\Sigma}_{Cq}; & -v^{\Delta}_{Cd} - v^{\Delta}_{CZ_d}; v^{\Delta}_{Cq} + v^{\Delta}_{CZ_q}; -v^{\Delta}_{Cd} \\ v^{\Sigma}_{Cq}; & v^{\Sigma}_{Cd} - 2v^{\Sigma}_{Cz}; & v^{\Delta}_{Cq} - v^{\Delta}_{CZ_q}; & v^{\Delta}_{Cd} - v^{\Delta}_{CZ_d}; 2v^{\Delta}_{Cq} \end{bmatrix}. \tag{11}$$

2.2.2 Common-mode arm currents

Similarly, applying the Park's transformation at -2ω to (2), the dynamics of the common-mode arm currents in their time invariant representation $\boldsymbol{i}^{\boldsymbol{\Sigma}}_{\boldsymbol{dq}}$ and i^{Σ}_{z} are obtained, shown in (12).

$$\begin{aligned} L_{arm} \frac{d\boldsymbol{i}^{\boldsymbol{\Sigma}}_{\boldsymbol{dq}}}{dt} &= -\boldsymbol{v}^{\boldsymbol{\Sigma}}_{\boldsymbol{mdq}} - R_{arm} \boldsymbol{i}^{\boldsymbol{\Sigma}}_{\boldsymbol{dq}} - 2\boldsymbol{J}_{\omega} L_{arm}\, \boldsymbol{i}^{\boldsymbol{\Sigma}}_{\boldsymbol{dq}} \\ L_{arm} \frac{di^{\Sigma}_{z}}{dt} &= -v^{\Sigma}_{mz} - R_{arm} i^{\Sigma}_{z} + \frac{v_{dc}}{2} \end{aligned} \tag{12}$$

with v_{dc} representing the voltage at the MMC DC terminals. The modulated voltages driving the currents $\boldsymbol{i}^{\boldsymbol{\Sigma}}_{\boldsymbol{dq}}$ and i^{Σ}_{z} are $\boldsymbol{v}^{\boldsymbol{\Sigma}}_{\boldsymbol{mdq}}$ and v^{Σ}_{mz}. These voltages are defined in (13), as a function of the modulation indexes:

$$\boldsymbol{v}^{\boldsymbol{\Sigma}}_{\boldsymbol{mdqz}} = \frac{1}{4} \boldsymbol{V}^{\boldsymbol{\Sigma}} \left[\boldsymbol{m}^{\boldsymbol{\Delta}}_{\boldsymbol{dq}}, \boldsymbol{m}^{\boldsymbol{\Sigma}}_{\boldsymbol{dq}}, m^{\Sigma}_{z} \right]^{\top}, \tag{13}$$

and $\boldsymbol{V}^{\boldsymbol{\Sigma}}$, the following 3×5 voltage matrix:

$$\boldsymbol{V}^{\boldsymbol{\Sigma}} \stackrel{\text{def}}{=} \begin{bmatrix} v^{\Delta}_{Cd} + v^{\Delta}_{CZ_d} & -v^{\Delta}_{Cq} + v^{\Delta}_{CZ_q} & 2v^{\Sigma}_{Cz} & 0 & v^{\Sigma}_{Cd} \\ -v^{\Delta}_{Cq} - v^{\Delta}_{CZ_q} & -v^{\Delta}_{Cd} + v^{\Delta}_{CZ_d} & 0 & 2v^{\Sigma}_{Cz} & 2v^{\Sigma}_{Cq} \\ v^{\Delta}_{Cd} & v^{\Delta}_{Cq} & v^{\Sigma}_{Cd} & v^{\Sigma}_{Cq} & 2v^{\Sigma}_{Cz} \end{bmatrix}. \tag{14}$$

2.2.3 Arm voltages sum

Applying the Park transformation at -2ω to (6), the time invariant dynamics of the voltage sum vector $\boldsymbol{v}^{\boldsymbol{\Sigma}}_{\boldsymbol{Cdqz}}$ result in (15).

$$C_{arm} \frac{d\boldsymbol{v}^{\boldsymbol{\Sigma}}_{\boldsymbol{Cdqz}}}{dt} = \boldsymbol{i}^{\boldsymbol{\Sigma}}_{\boldsymbol{mdqz}} - \begin{bmatrix} 2\boldsymbol{J}_{\omega} & \boldsymbol{0}_{2\times 1} \\ \boldsymbol{0}_{1\times 2} & 0 \end{bmatrix} C_{arm} \boldsymbol{v}^{\boldsymbol{\Sigma}}_{\boldsymbol{Cdqz}} \tag{15}$$

with $\boldsymbol{i}^{\boldsymbol{\Sigma}}_{\boldsymbol{mdqz}}$ representing the modulated current as defined in (16), as a function of the modulation indexes,

$$\boldsymbol{i}^{\boldsymbol{\Sigma}}_{\boldsymbol{mdqz}} = \frac{1}{8} \boldsymbol{I}^{\Sigma} \left[\boldsymbol{m}^{\boldsymbol{\Delta}}_{\boldsymbol{dq}}, \boldsymbol{m}^{\boldsymbol{\Sigma}}_{\boldsymbol{dq}}, m^{\Sigma}_{z} \right]^{\top} \tag{16}$$

and $I^{\boldsymbol{\Sigma}}$, the following 3×5 time invariant current matrix:

$$I^{\boldsymbol{\Sigma}} \stackrel{\text{def}}{=} \begin{bmatrix} i^{\Delta}_{d} & -i^{\Delta}_{q} & 4i^{\Sigma}_{z} & 0 & 4i^{\Sigma}_{d} \\ i^{\Delta}_{q} & -i^{\Delta}_{d} & 0 & -4i^{\Sigma}_{z} & -4i^{\Sigma}_{q} \\ i^{\Delta}_{d} & i^{\Delta}_{q} & 2i^{\Sigma}_{d} & 2i^{\Sigma}_{q} & 4i^{\Sigma}_{z} \end{bmatrix}. \tag{17}$$

2.2.4 Arm voltages difference

Finally, the steady-state time invariant dynamics of the voltage difference vectors $\boldsymbol{v}^{\boldsymbol{\Delta}}_{\boldsymbol{Cdq}}$ and v^{Δ}_{CZ} are now recalled. Results are obtained by applying the Park's transformation at ω and 3ω to (7). For the sake of compactness, the voltage difference vector is defined as $\boldsymbol{v}^{\boldsymbol{\Delta}}_{\boldsymbol{CdqZ}} \stackrel{\text{def}}{=} \left[v^{\Delta}_{Cd}, v^{\Delta}_{Cq}, v^{\Delta}_{CZ_d}, v^{\Delta}_{CZ_q} \right]^{\top}$.

This is the accepted version of a paper published in 13th IET International Conference on AC and DC Power Transmission - ACDC 2017
DOI: 10.1049/cp.2017.0016

$$C_{arm}\frac{d\boldsymbol{v}^{\boldsymbol{\Delta}}_{\boldsymbol{CdqZ}}}{dt} = \boldsymbol{i}^{\boldsymbol{\Delta}}_{\boldsymbol{mdqZ}} - \begin{bmatrix} \boldsymbol{J}_\omega & \boldsymbol{0}_{2\times 2} \\ \boldsymbol{0}_{2\times 2} & 3\boldsymbol{J}_\omega \end{bmatrix} C_{arm}\boldsymbol{v}^{\boldsymbol{\Delta}}_{\boldsymbol{CdqZ}} \quad (18)$$

with $\boldsymbol{i}^{\boldsymbol{\Delta}}_{\boldsymbol{mdqZ}}$ representing the modulated current as defined in (19), as a function of the modulation indexes,

$$\boldsymbol{i}^{\boldsymbol{\Delta}}_{\boldsymbol{mdqZ}} = \frac{1}{8} I^{\boldsymbol{\Delta}} \left[\boldsymbol{m}^{\boldsymbol{\Delta}}_{\boldsymbol{dq}}, \boldsymbol{m}^{\boldsymbol{\Sigma}}_{\boldsymbol{dq}}, m^{\Sigma}_{z}\right]^{\top} \quad (19)$$

and $I^{\boldsymbol{\Delta}}$, the following 4×5 time-invariant current matrix:

$$I^{\boldsymbol{\Delta}} \stackrel{\text{def}}{=} \begin{bmatrix} 2i^{\Sigma}_d + 4i^{\Sigma}_z & -2i^{\Sigma}_q & i^{\Delta}_d & -2i^{\Delta}_q & 2i^{\Delta}_d \\ -2i^{\Sigma}_q & -2i^{\Sigma}_d + 4i^{\Sigma}_z & -i^{\Delta}_q & -i^{\Delta}_d & 2i^{\Delta}_q \\ 2i^{\Sigma}_d & 2i^{\Sigma}_q & i^{\Delta}_d & i^{\Delta}_q & 0 \\ -2i^{\Sigma}_q & 2i^{\Sigma}_d & i^{\Delta}_q & -i^{\Delta}_d & 0 \end{bmatrix}. \quad (20)$$

2.2.5 DC bus dynamics

The DC bus dynamics are modelled by (21), where C_{dc} is the cable model terminal capacitance and P_l represents the power injection as seen from the MMC station.

$$C_{dc}\frac{dv_{dc}}{dt} = -\frac{P_l}{v_{dc}} - 3i^{\Sigma}_z \quad (21)$$

An overview of the model structure corresponding to the MMC and DC bus equations is shown in Fig. 2.

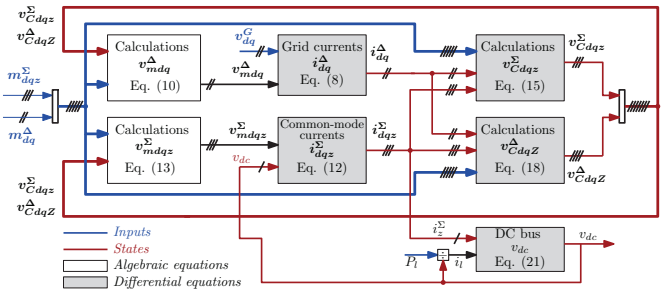

Figure 2: MMC and DC bus equations resume

3 DC voltage droop control and circulating current suppressing controller

The MMC control structure is shown in Fig. 3. For the AC-side the MMC control strategy is based on a classical scheme with two cascaded loops. The outer loop controls the active power P_{ac} following a P_{ac}—v_{dc} droop characteristic with gain k_d [17].

The inner loops control the AC currents in SRF. The variables $v^{\Delta *}_{md}$ and $v^{\Delta *}_{mq}$ are the output of the controllers regulating the grid side current $\boldsymbol{i}^{\boldsymbol{\Delta}}_{\boldsymbol{dq}}$ to the desired reference $\boldsymbol{i}^{\boldsymbol{\Delta *}}_{\boldsymbol{dq}}$ by implementing standard SRF current controllers with decoupling feed-forward terms, as briefly recalled in (22).

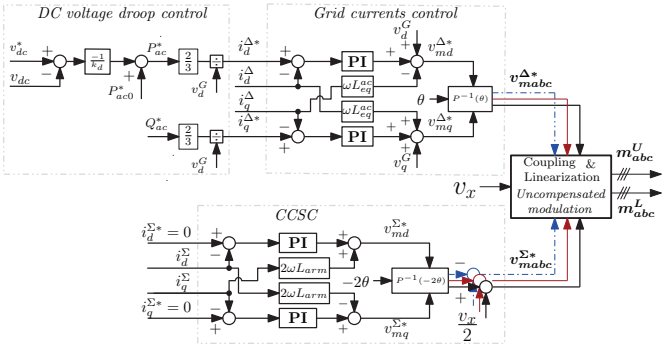

Figure 3: MMC droop-controlled with CCSC

$$\frac{d\boldsymbol{\xi}^{\boldsymbol{\Delta}}_{\boldsymbol{dq}}}{dt} = \left(\boldsymbol{i}^{\boldsymbol{\Delta *}}_{\boldsymbol{dq}} - \boldsymbol{i}^{\boldsymbol{\Delta}}_{\boldsymbol{dq}}\right) \quad (22)$$
$$\boldsymbol{v}^{\boldsymbol{\Delta *}}_{\boldsymbol{mdq}} = K^{\Delta}_{p}\left(\boldsymbol{i}^{\boldsymbol{\Delta *}}_{\boldsymbol{dq}} - \boldsymbol{i}^{\boldsymbol{\Delta}}_{\boldsymbol{dq}}\right) + \frac{1}{T^{\Delta}_{i}}\boldsymbol{\xi}^{\boldsymbol{\Delta}}_{\boldsymbol{dq}} - \boldsymbol{J}\omega L^{ac}_{eq}\boldsymbol{i}^{\boldsymbol{\Delta}}_{\boldsymbol{dq}} + \boldsymbol{v}^{\boldsymbol{G}}_{\boldsymbol{dq}}$$

Furthermore, $v^{\Sigma *}_{md}$ and $v^{\Sigma *}_{mq}$ are the outputs of the CCSC regulators [15], as given in (23), forcing the circulating currents $\boldsymbol{i}^{\boldsymbol{\Sigma}}_{\boldsymbol{dq}}$ to zero ($\boldsymbol{0}_{2\times 1}$). The output DC current of the converter is left uncontrolled and it is naturally adjusted to balance the AC and DC power [3].

$$\frac{d\boldsymbol{\xi}^{\boldsymbol{\Sigma}}_{\boldsymbol{dq}}}{dt} = \left(\boldsymbol{0}_{2\times 1} - \boldsymbol{i}^{\boldsymbol{\Sigma}}_{\boldsymbol{dq}}\right) \quad (23)$$
$$\boldsymbol{v}^{\boldsymbol{\Sigma *}}_{\boldsymbol{mdq}} = K^{\Sigma}_{p}\left(\boldsymbol{0}_{2\times 1} - \boldsymbol{i}^{\boldsymbol{\Sigma}}_{\boldsymbol{dq}}\right) + \frac{1}{T^{\Sigma}_{i}}\boldsymbol{\xi}^{\boldsymbol{\Sigma}}_{\boldsymbol{dq}} + 2\boldsymbol{J}\omega L_{arm}\boldsymbol{i}^{\boldsymbol{\Sigma}}_{\boldsymbol{dq}}$$

The MMC insertion indexes are calculated directly from the output of the control loops for the ac-side and circulating current suppressing controller as shown in (24). This calculation of the insertion indexes will be referred to as the "Un-Compensated Modulation" (UCM) [14] since there is no compensation for neither the steady-state oscillations nor the dynamic dynamic variations in the equivalent capacitor voltages.

$$m^{U}_{j} = \frac{-v^{\Delta *}_{mj} - v^{\Sigma *}_{mj}}{v_x} + \frac{1}{2}, \quad m^{L}_{j} = \frac{v^{\Delta *}_{mj} - v^{\Sigma *}_{mj}}{v_x} + \frac{1}{2} \quad (24)$$

With the definitions of m^{Σ}_{j} and m^{Δ}_{j} from Section 2 and taking into account (24), the modulation indexes in SRF can be obtained as in (25),

$$m^{\Sigma}_{d} = -2\frac{v^{\Sigma *}_{md}}{v_x}, \quad m^{\Sigma}_{q} = -2\frac{v^{\Sigma *}_{mq}}{v_x}, \quad m^{\Sigma}_{z} = 1$$
$$m^{\Delta}_{d} = -2\frac{v^{\Delta *}_{md}}{v_x}, \quad m^{\Delta}_{q} = -2\frac{v^{\Delta *}_{mq}}{v_x} \quad (25)$$

This is the accepted version of a paper published in 13th IET International Conference on AC and DC Power Transmission - ACDC 2017
DOI: 10.1049/cp.2017.0016

The variable v_x in (24) and (25) can be replaced by the measure of v_{dc}, or its nominal value $v_{dc,nom}$. It will be shown by the small-signal eigenvalue analysis that this choice can influence the dynamics and stability of the studied system

The control presented in this section will be referred as *non-energy based* control since the internal stored energy is not being controlled explicitly. When the *non-energy based* control strategy is applied, the average value of the equivalent arm capacitor voltages v_{Cj}^{U} and v_{Cj}^{L} follows the DC bus voltage v_{dc}. Hence, for slow transients it can be considered that there is a capacitor connected to the DC bus with value $6 \times C_{arm}$ [3, 17].

4 Model linearization and time domain validation

The non-linear SSTI model presented in the Section 2 with the control from Section 3 can be linearised around a steady-state operating point. This linearised model is used for evaluating small-signal dynamics and stability by eigenvalue analysis but the detail model is not shown due to lack of space.

To validate the developed small-signal model of the MMC with *Non-energy based* control, results from simulation of three different models will be shown and discussed in the following:

1. *EMT*: The system from Fig. 1 implemented in EMTP-RV. The MMC is modeled with the so-called "Model # 3: *Arm Switching Function*" from [16]. The considered controller is from Fig. 3.
2. *Simp*: Non-linear time-invariant model implemented in Matlab/Simulink. This model represents the equations resumed in Fig. 2 with the controller in SRF from Fig. 3 and the modulation indexes from (25).
3. *StSp*: linearised time-invariant model from the *Simp* model implemented in Matlab/Simulink.

The main system parameters are listed in Table 2.

U_{1n}	320[kV]	R_f	0.521[Ω]	T_i^{Δ}	4.7×10^{-3}
f_n	50[Hz]	L_f	58.7[mH]	K_p^{Δ}	34.9
N	400[-]	R_{arm}	1.024[Ω]	T_i^{Σ}	2.3×10^{-3}
C_{arm}	32.55[μF]	L_{arm}	48[mH]	K_p^{Σ}	41.07
C_{dc}	195.3[μF]	v_{dcn}	640[kV]	k_d	0.1[pu]

Table 2: Parameters for the time domain simulation

Starting with a DC power transfer of 1pu (from DC to AC), a step is applied on P_l of -0.1[pu]. The reactive power is controlled to zero during the event. Simulation results are gathered in Fig. 4.

Figure 4(a) shows the results of the DC powers. Since the DC power is a non-linear relation between states, the results for P_{dc} of the linear model is post-processed as $P_{dc} = 3i_z^{\Sigma}v_{dc}$.

The step applied on P_l produces power imbalance in the DC bus, and the MMC reacts with the droop controller and its internal energy to achieve the new equilibrium point. The DC voltage resulting from the different models are shown in Fig. 4(c). The DC bus voltage deviation is defined by the droop parameter k_d. The internal energy of the MMC participates in the dynamics of the DC voltage regulation by discharging its internal capacitors into the DC bus during the transients, as seen in the voltage v_{Cz}^{Σ} from Fig. 4(d). The behavior of v_{Cz}^{Σ} is similar to the DC bus voltage. This is the reason that it can be considered that the equivalent DC bus capacitance C_{dc} is reinforced with $6 \times C_{arm}$ as discussed in [17].

Finally, the results of the differential currents are shown in Fig. 4(b) (only dq components). The EMT model presents oscillations at 6ω in steady state. This oscillations were neglected during the development of the time-invariant model [14]. As seen in the comparisons from Fig. 4, the model captures the average dynamics with reasonable accuracy even if the 6^{th} harmonic components are ignored. For all other variables, there are negligible differences between the different models.

5 Small signal stability analysis of a droop-controlled MMC connected to a DC bus

In this section, the small-signal dynamics and stability of the linearised model are studied. The impact of two main parameters influencing the DC voltage dynamics are evaluated: the DC capacitor value and the droop parameters [17]. Moreover, the effect of the choice in the modulation index calculation from (24) and (25) is evaluated, i.e. division by the measured value of v_{dc}, or a constant value $v_{dc,nom}$.

5.1 Influence of the DC capacitor

The electrostatic constant H_{dc} is defined as,

$$H_{dc} = \frac{1}{2} C_{dc} \frac{v_{dcn}^2}{P_n}. \tag{26}$$

The value of H_{dc} is varied from 40ms down to 5ms. This last value represents a small equivalent capacitance of the DC bus ($24,4\mu F << (6 \times C_{arm})$).

5.1.1 Active power from DC to AC sides

The first results considers a power direction from DC to AC side of 1GW of power transfer. Results are shown in Fig. 5. The eigenvalues trajectories for the parametric sweep of H_{dc} in the case of the modulation with measured v_{dc} is shown in Fig. 5(a). In this case, for the selected values the system remains stable.

When the modulation indexes are calculated with a constant value (e.g. $v_{dc,nom}$), the results varies as depicted in Fig. 5(b). The trajectories of the eigenvalues are similar as in Fig. 5(a), but in this case, an instability is observed when the value of H_{dc} is near 20ms, since the the pair of eigenvalues $\lambda_{1,2}$ shift to the right hand plane.

For validating the results, a new time-domain simulation is performed with a DC capacitor of $97,65\mu$F. The simulated

This is the accepted version of a paper published in 13th IET International Conference on AC and DC Power Transmission - ACDC 2017
DOI: 10.1049/cp.2017.0016

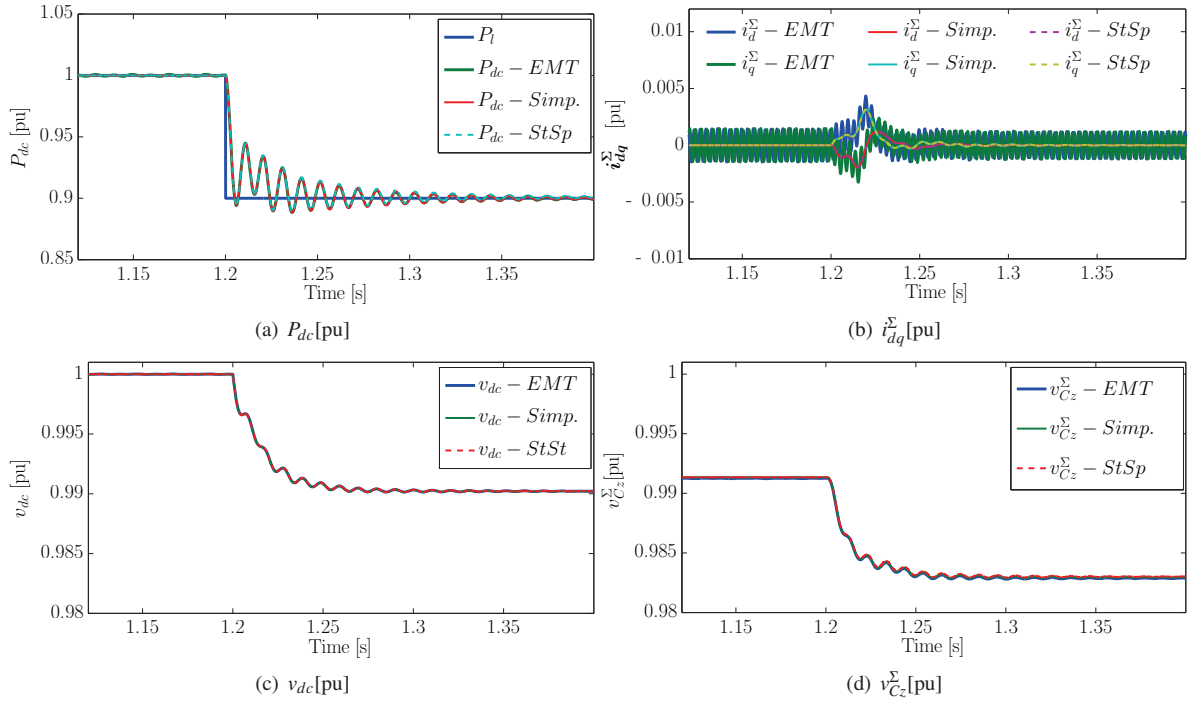

(a) P_{dc}[pu] (b) i_{dq}^Σ[pu]

(c) v_{dc}[pu] (d) v_{Cz}^Σ[pu]

Figure 4: Time domain validation – Step applied on P_l of 0.1pu – *EMT*: EMTP-RV simulation, *Simp.*: Non-linear time-invariant model in Simulink, *StSp*: Linear time-invariant state-space model in Simulink

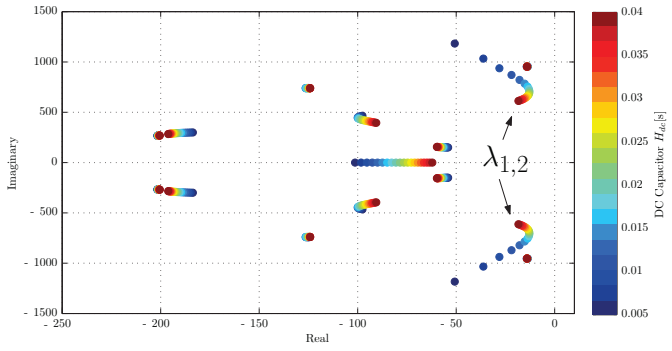

(a) Modulation index calculated with measured v_{dc}

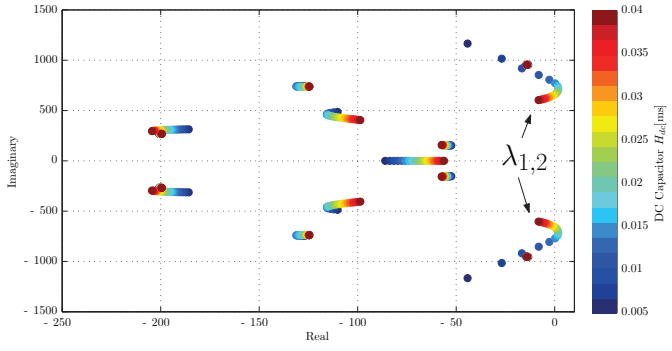

(b) Modulation index calculated with nominal value $v_{dc,nom}$

Figure 5: Parametric sweep of DC capacitor H_{dc} — DC Operating point $v_{dc0} = 1$[pu], $P_{dc0} = 1$[pu] — $k_d = 0.1$pu

event is similar to the previous section. Results are shown in Fig. 6, where the instability is clearly highlighted. For the *EMT* model, the simulation is started with two capacitors in parallel on the DC side, one of $97,65\mu$F and one with value 195μF. At $t = 1.15$s the larger capacitor is disconnected, resulting in a DC bus capacitance of $97,65\mu$F, i.e. the unstable value. The frequency of the oscillations is approximately 110Hz.

5.1.2 Active power from AC to DC sides

It is known that the converters dynamics depend on the operating point [18]. The same parametric sweep as the previous section is performed with the opposite power transfer direction (i.e. from AC to DC side). Results are shown in Fig. 7(a) and 7(b) for the modulation index calculated with measured v_{dc} or $v_{dc,nom}$ respectively. For both cases, when the DC capacitor decreases the system is unstable. When the measured voltage is used for the modulation index, the system can support lower values of DC capacitor than for the constant value.

5.2 Influence of the droop parameter

In this case, the droop parameter k_d is varied from 0.2pu down to 0.05pu. The considered power direction is from AC to DC sides since it is the worst case from previous section. Results are shown in 8. For both cases when lower values of droop are used, the eigenvalues $\lambda_{1,2}$ shift to the right-hand plane resulting in unstable behavior. Nevertheless, it is observed that in Fig. 8(a) the droop parameter k_d that makes the system unstable is lower than for Fig. 8(b).

This is the accepted version of a paper published in 13th IET International Conference on AC and DC Power Transmission - ACDC 2017
DOI: 10.1049/cp.2017.0016

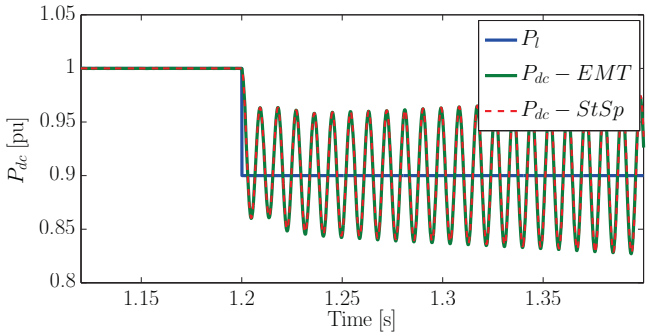

(a) P_{dc}[pu]

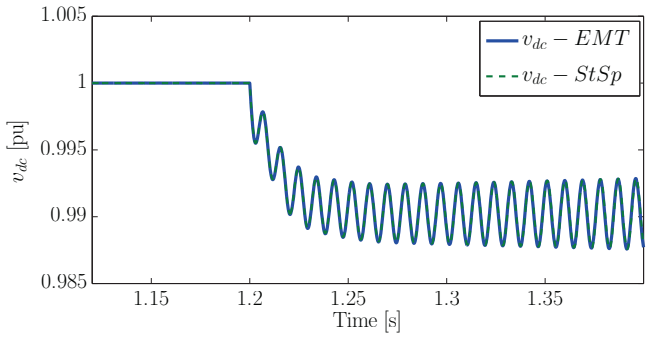

(b) v_{dc}[pu]

Figure 6: Instability verification with time-domain simulation — Modulation index calculated with nominal value $v_{dc,nom}$

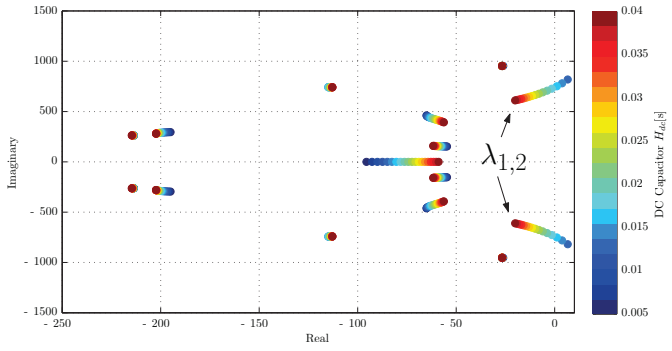

(a) Modulation index calculated with measured v_{dc}

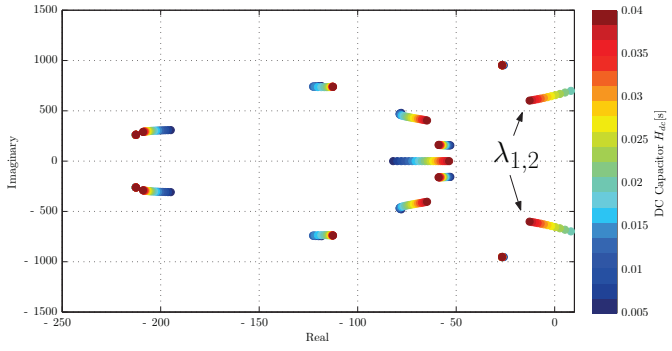

(b) Modulation index calculated with nominal value $v_{dc,nom}$

Figure 7: Parametric sweep of DC capacitor H_{dc} — DC Operating point $v_{dc0} = 1$[pu], $P_{dc0} = -1$[pu] — $k_d = 0.1$pu

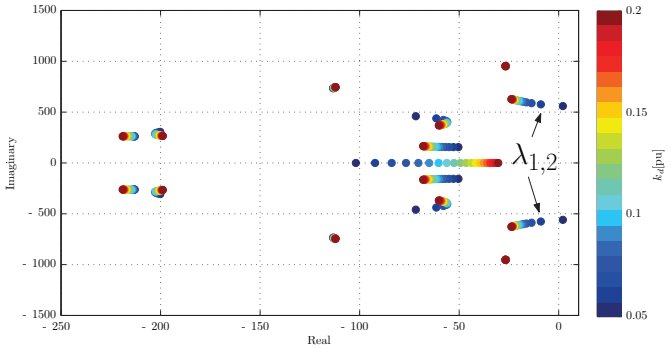

(a) Modulation index calculated with measured v_{dc}

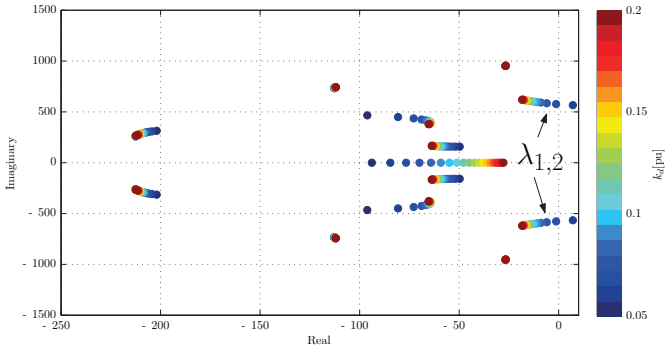

(b) Modulation index calculated with nominal value $v_{dc,nom}$

Figure 8: Parametric sweep of Droop parameter k_d — DC Operating point $v_{dc0} = 1$[pu], $P_{dc0} = -1$[pu]

5.3 Identification of unstable eigenvalues

As observed in the previous results (Fig. 5 to Fig. 8), the system may become unstable due to the same pair of eigenvalues for all cases ($\lambda_{1,2}$). For understanding the origin of these eigenvalues, the participation factor analysis is performed and the results are shown in Fig. 9. The considered case corresponds to the operating point and parameters from Section 4.

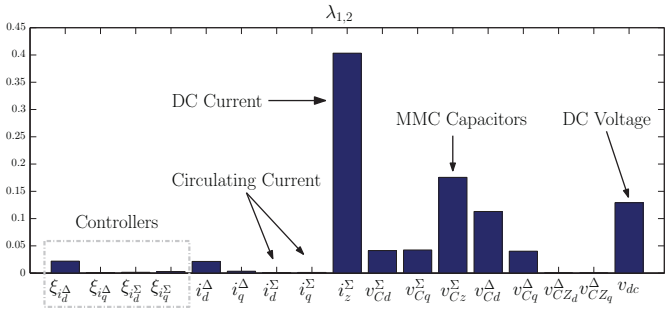

Figure 9: Results from participation factor analysis - Eigenvalues $\lambda_{1,2}$

Fig. 9 indicates that the states with the highest participation in the low-frequency oscillatory mode are i_z^Σ (i.e. the DC current), v_{Cz}^Σ (the state of the MMC which represents the internal energy) and v_{dc} (DC voltage). It indicates also that the controller (with the chosen bandwidths) don't have significant influence on these

This is the accepted version of a paper published in 13th IET International Conference on AC and DC Power Transmission - ACDC 2017
DOI: 10.1049/cp.2017.0016

eigenvalues and neither do the internal circulating currents $\boldsymbol{i}_{dq}^{\Sigma}$.

6 Conclusions

This paper presented a small signal model of a droop-controlled MMC with CCSC connected to a DC power source and an equivalent capacitance. The resulting model was validated against EMT simulations. The presented detailed small signal model of the MMC with SSRF may be extended to other control methods where the internal stored energy (and the DC current) are explicitly controlled. The small signal analysis suggests that the calculations of the modulation indexes with the measured DC voltage enhances the stability of the system. Moreover, the studied system has shown that the active power flow direction has an effect on the stability margin. This phenomenon will have a large impact on multiterminal DC grids.

By means of modal analysis and participation factors, it was shown that the observed instabilities are directly related with the uncontrolled DC (output) current of the MMC. This indicates that closed loop control of the DC current can be beneficial for the small-signal stability of an MMC-based HVDC terminal.

Appendix

A. Park Transformation

$$\boldsymbol{P}_{n\omega} = \frac{2}{3}\begin{bmatrix} cos(n\omega t) & cos(n\omega t - \frac{2\pi}{3}) & cos(n\omega t - \frac{4\pi}{3}) \\ sin(n\omega t) & sin(n\omega t - \frac{2\pi}{3}) & sin(n\omega t - \frac{4\pi}{3}) \\ \frac{1}{2} & \frac{1}{2} & \frac{1}{2} \end{bmatrix} \quad (27)$$

References

[1] A. Lesnicar and R. Marquardt, "An innovative modular multilevel converter topology suitable for a wide power range," in *Power Tech Conference Proceedings, 2003 IEEE Bologna*, vol. 3, pp. 6 pp. Vol.3–, June 2003.

[2] A. Antonopoulos, L. Angquist, and H. P. Nee, "On dynamics and voltage control of the modular multilevel converter," in *Power Electronics and Applications, 2009. EPE '09. 13th European Conference on*, pp. 1–10, Sept 2009.

[3] L. Harnefors, A. Antonopoulos, S. Norrga, L. Angquist, and H.-P. Nee, "Dynamic analysis of modular multilevel converters," *Industrial Electronics, IEEE Transactions on*, vol. 60, pp. 2526–2537, July 2013.

[4] J. Beerten, S. D'Arco, and J. A. Suul, "Identification and small-signal analysis of interaction modes in vsc mtdc systems," *IEEE Transactions on Power Delivery*, vol. 31, pp. 888–897, April 2016.

[5] P. Rault, F. Colas, X. Guillaud, and S. Nguefeu, "Method for small signal stability analysis of vsc-mtdc grids," in *Power and Energy Society General Meeting, 2012 IEEE*, pp. 1–7, July 2012.

[6] N. R. Chaudhuri, R. Oliveira, and A. Yazdani, "Stability analysis of vector-controlled modular multilevel converters in linear time-periodic framework," *IEEE Transactions on Power Electronics*, vol. 31, pp. 5255–5269, July 2016.

[7] P. Kundur, N. J. Balu, and M. G. Lauby, *Power system stability and control*. McGraw-hill New York, 1994.

[8] S. Liu, Z. Xu, W. Hua, G. Tang, and Y. Xue, "Electromechanical transient modeling of modular multilevel converter based multi-terminal hvdc systems," *IEEE Transactions on Power Systems*, vol. 29, pp. 72–83, Jan 2014.

[9] D. C. Ludois and G. Venkataramanan, "Simplified terminal behavioral model for a modular multilevel converter," *IEEE Transactions on Power Electronics*, vol. 29, pp. 1622–1631, April 2014.

[10] N. T. Trinh, M. Zeller, K. Wuerflinger, and I. Erlich, "Generic model of mmc-vsc-hvdc for interaction study with ac power system," *IEEE Transactions on Power Systems*, vol. 31, pp. 27–34, Jan 2016.

[11] J. Freytes, L. Papangelis, H. Saad, P. Rault, T. V. Cutsem, and X. Guillaud, "On the modeling of mmc for use in large scale dynamic simulations," in *2016 Power Systems Computation Conference (PSCC)*, pp. 1–7, June 2016.

[12] G. Bergna Diaz, J. A. Suul, and S. D'Arco, "Small-signal state-space modeling of modular multilevel converters for system stability analysis," in *Energy Conversion Congress and Exposition (ECCE), 2015 IEEE*, pp. 5822–5829, Sept 2015.

[13] A. Far and D. Jovcic, "Small signal dynamic dq model of modular multilevel converter for system studies," *Power Delivery, IEEE Transactions on*, vol. PP, no. 99, pp. 1–1, 2015.

[14] G. Bergna, J. A. Suul, and S. D'Arco, "State-space modelling of modular multilevel converters for constant variables in steady-state," in *2016 IEEE 17th Workshop on Control and Modeling for Power Electronics (COMPEL)*, pp. 1–9, June 2016.

[15] Q. Tu, Z. Xu, and J. Zhang, "Circulating current suppressing controller in modular multilevel converter," in *IECON 2010 - 36th Annual Conference on IEEE Industrial Electronics Society*, pp. 3198–3202, Nov 2010.

[16] H. Saad, S. DennetieÌĂre, J. Mahseredjian, P. Delarue, X. Guillaud, J. Peralta, and S. Nguefeu, "Modular multilevel converter models for electromagnetic transients," *Power Delivery, IEEE Transactions on*, vol. 29, pp. 1481–1489, June 2014.

[17] J. Freytes, P. Rault, F. Colas, F. Gruson, and X. Guillaud, "Dynamic impact of mmc controllers on dc voltage droop controlled mtdc grids," in *18th European Conference on Power Electronics and Applications (EPE)*, 2016.

[18] J. Freytes, S. Akkari, J. Dai, F. Gruson, P. Rault, and X. Guillaud, "Small-signal state-space modeling of an hvdc link with modular multilevel converters," in *2016 IEEE 17th Workshop on Control and Modeling for Power Electronics (COMPEL)*, pp. 1–8, June 2016.

This is the accepted version of a paper published in 13th IET International Conference on AC and DC Power Transmission - ACDC 2017
DOI: 10.1049/cp.2017.0016